Electronic Supplementary Material (ESI) for Journal of Materials Chemistry A.

Supplementary Information

Symmetry-induced Modulation of Proton Conductivity in Y-doped $Ba(Zr,Ce)O_3$: Insights from Raman Spectroscopy

Yiming Yang‡[1], Jiachen Lu‡[1], Xinyu Zhang[2], Yanuo Shi[2], Peng Du[1], Xiao Ling[1], Nan Yang[2,*], Qianli Chen[1,*]

1. University of Michigan – Shanghai Jiao Tong University Joint Institute, Shanghai Jiao Tong University, Shanghai 200240, China. E-mail: qianli.chen@sjtu.edu.cn

2. School of Physical Science and Technology, ShanghaiTech University, Shanghai 201210, China. E-mail: yangnan@shanghaitech.edu.cn

‡ Equal contribution.

1. Proton conductivity of ceramic thin films

Table S1. Summary of the conductivity of Y-doped $BaZrO_3$ (BZY) proton conducting epitaxial thin films reported in literature.

Component /Substrate	Thickness	Conductivity ($S \cdot cm^{-1}$)	Temperature (℃)	E_a (eV)	Reference
BZY/MgO	60 nm	2.8×10^{-3} at 250 °C	140-290	0.44	Shim et al.[1]
BZY/MgO	120 nm	1.1×10^{-2} at 400 °C	150-350	0.45	Kim et al.[2]
BZY/MgO	73nm	/	180-380	0.47	Fluri et al.[3]
BZY/MgO	1 μm	0.11 at 500 °C	350-650	0.63	Pergolesi et al.[4]
BZY/MgO	500nm	0.015 at 500 °C	300–600	1.03	Bae et al.[5]
BZY/MgO	100nm	5×10^{-5} at 530 °C	300-630	0.8	Foglietti et al.[6]
BZY/MgO	200nm	4.1×10^{-3} at 500 °C	350-650	0.88	Wang et al.[7]

2. Raman data processing methodology

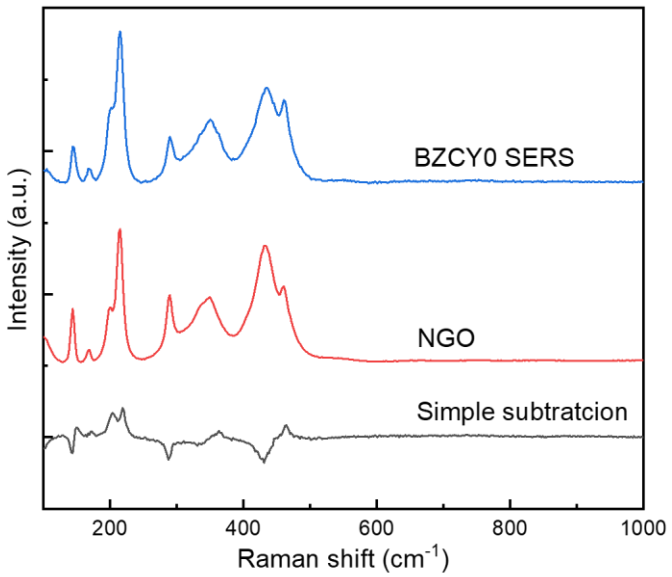

Figure S1. SERS spectra of the BZCY0 thin film, NGO substrate, and the outcome of subtracting the spectrum of thin film from the NGO substrate.

Nonnegative Matrix Factorization (NMF) method

The data were organized as columns of matrix V. The matrices V were decomposed by principal component analysis (PCA) giving elementwise matrices H and W that V=WH+E. The error matrix E contains the noise information and the matrix V=WH is the resulting smoothed data. The columns of matrix W are the basis functions (the spectra of substrate and film) and rows of matrix H are the corresponding linear coefficients ascribing the weight of the basis function in each experimental spectrum. The matrices W and H are therefore of rank n×k and k×m, respectively, where k is the number of basis functions, n is the number of data points in each experimental spectrum, and m is the number of experimental spectra. The number of k is determined by the number of largest singular values of the matrix V factorized by PCA and is widely used in hyperspectral data unmixing.

In this research, the raw data for analysis consists of a matrix "V" with 3 spectra from different samples (BZCY20, BZCY10 and BZCY0). The matrix V is factorized by NMF with rank k=2, giving two nonnegative basis functions (columns of matrix W). The first two principal components account for 99.99% of all data, as shown in Table S2. Figure S2 compares the SERS signals of the two columns with the SERS spectra of bare NGO substrate, and similar distribution was found between Raman peaks in the first column (denoted as NMF1) and NGO. The distribution of NMF1 represents the shared characteristics (substrate) of all thin film samples. The hit quality index (HQI) analysis was performed to identify the closeness between NMF1 and SERS spectra of bare NGO substrate.[8] A spectral similarity of 91.5% was obtained between NMF1 and the NGO substrate. Therefore, NMF1 is attributed to the substrate. The linear coefficients in Table S3 show the contributions of the substrate in different thin films.

Table S2. Cumulative Proportion of PCs

	PC1	PC2	PC3
Cumulative Proportion	0.9840	0.9996	0.9998

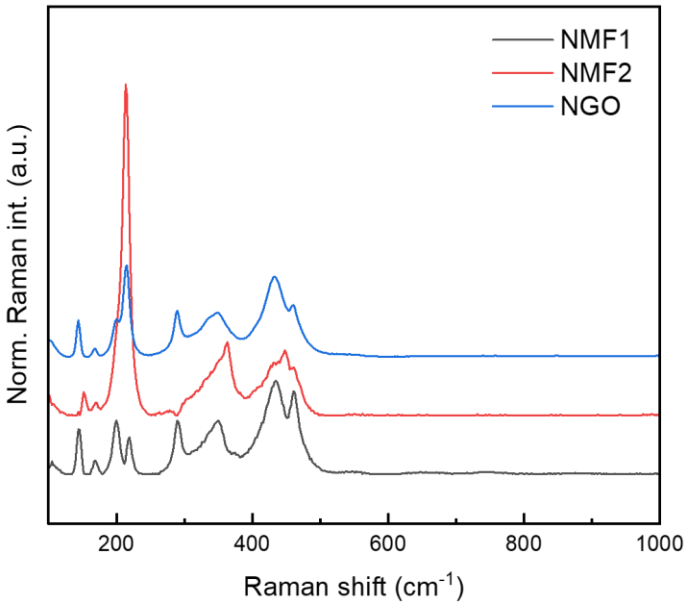

Figure S2. Comparison between NMF components from SERS spectra of thin films and SERS spectra of bare NGO. Red and black spectra are basis functions obtained by NMF. Blue, Raman spectra of bare NGO. All patterns were vertically shifted for comparison.

Table S3. The corresponding coefficients (contribution) of NMF1 (substrate) in different BZCY films

BZCY films	Linear coefficients
BZCY20	0.3536
BZCY10	0.5003
BZCY0	0.5246

Table S4. Enhancement factor of different samples

BZCY films	Enhancement factor
BZCY20	10.4
BZCY10	27.5
BZCY0	4.4

3. Determination of lattice volume for epitaxial films and bulk BZCY

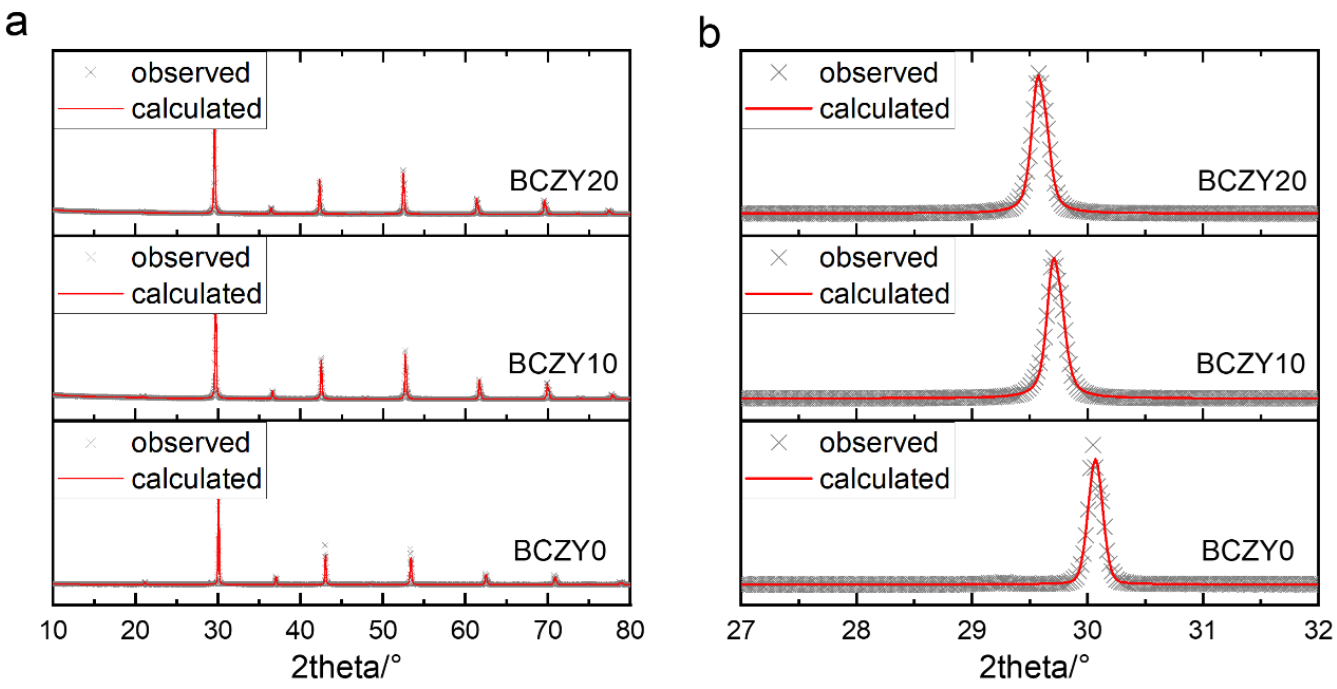

Figure S3. (a) Refined XRD pattern of bulk BZCY with different Ce content. (b) Zoom-in XRD pattern with 2theta from 27° to 32° of (110) peak. All patterns were vertically shifted for comparison.

The out-of-plane lattice constant (a_{out}, black squares) is directly calculated according to Bragg's equation, as shown in Figure S4a. The Poisson's ratio is defined as the deformation of a material in directions perpendicular to the specific direction of loading.

According to the expansion for an elastic body in the out-of-plane direction (σ_{out}, black squares in Figure S4a), in-plane strain (σ_{in}, red spheres in Figure S4b) can be inversely obtained by devising the Poisson's ratio of $BaZrO_3$ (v = 0.237 in this calculation[9]) following the equation $\sigma_{in} = \sigma_{out}/v$. The resulting in-plane lattice constant (a_{in}, blue triangles in Figure S4a) decreases with the increasing doping content. The biaxial strain is −5.0 ± 1.6%, −2.0 ± 1.6%, and −2.0 ± 1.6% for the BZCY0, BZCY10 and BZCY20 films, respectively.

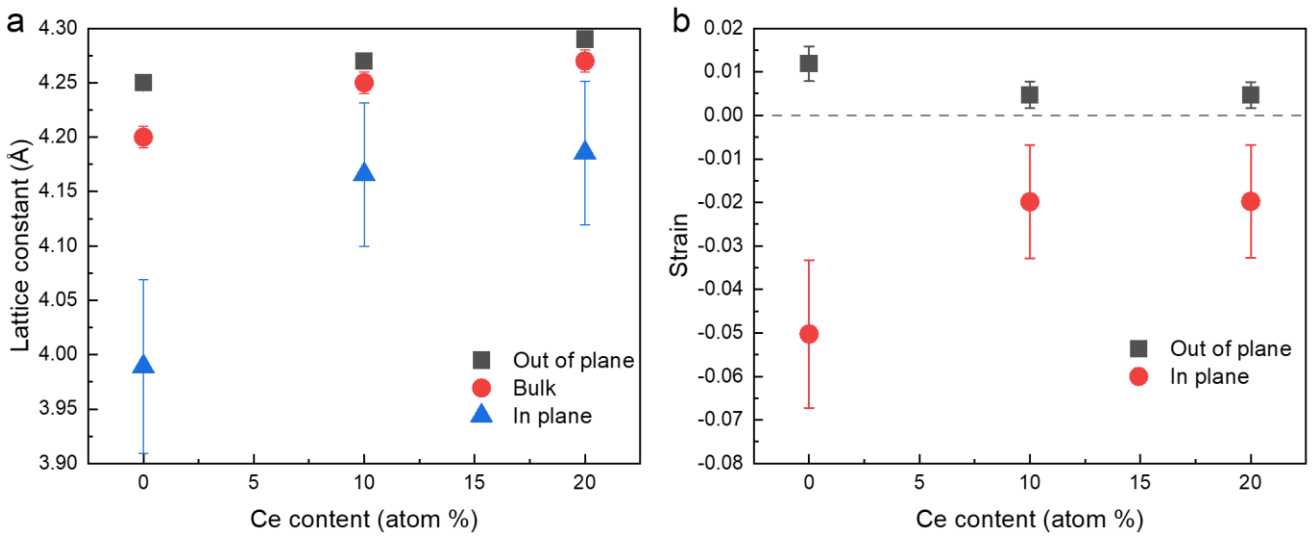

Figure S4. (a) Lattice constant of BZCY epitaxial films. Black squares, out-of-plane lattice constant calculated by Bragg's law. Blue triangles, in-plane lattice constant calculated according to Poisson's ratio (0.237 for undoped $BaZrO_3$[9]). Red circles, lattice constant of bulk BZCY obtained by Rietveld refinement. (b) Strain in BZCY films. Black squares, in-plane strain. Red circles, the biaxial in plane strain induced by the in-plane compression. Both the errors come from the XRD instrument error.

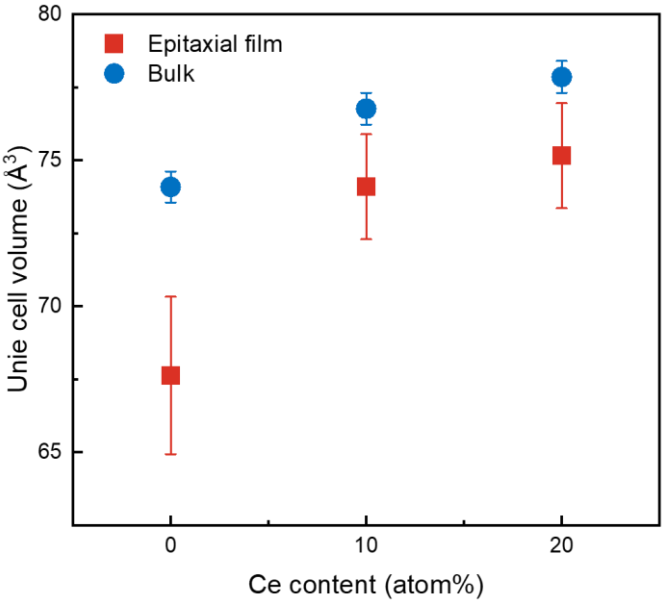

Figure S5. Estimated volume of epitaxial films and bulk BZCY. The errors originate from the calculated lattice constant in Figure S4a.

4. Raman spectra fitting and relative intensity

The peak analysis for the region of 200-800 cm^{-1} of bulk BZCY and BZCY films were accomplished using Lorentz functions, as displayed in Figure S6 and Figure S7. The fitting parameters including peak position, full width at half maximum (FWHM) and peak intensity (area) were all set free during fitting and the detailed results are listed in Table S5 and Table S6. Significant difference of the band width in these two BZCY samples may indicate the distinct distribution of the local defects, leading to different chemical environments surrounding the BO_6 octahedra, and thereof causing different levels of local symmetry. The existing grain boundaries in bulk BZCY may also increase the band width of Raman peaks, as reported in similar perovskite-type materials.[10]

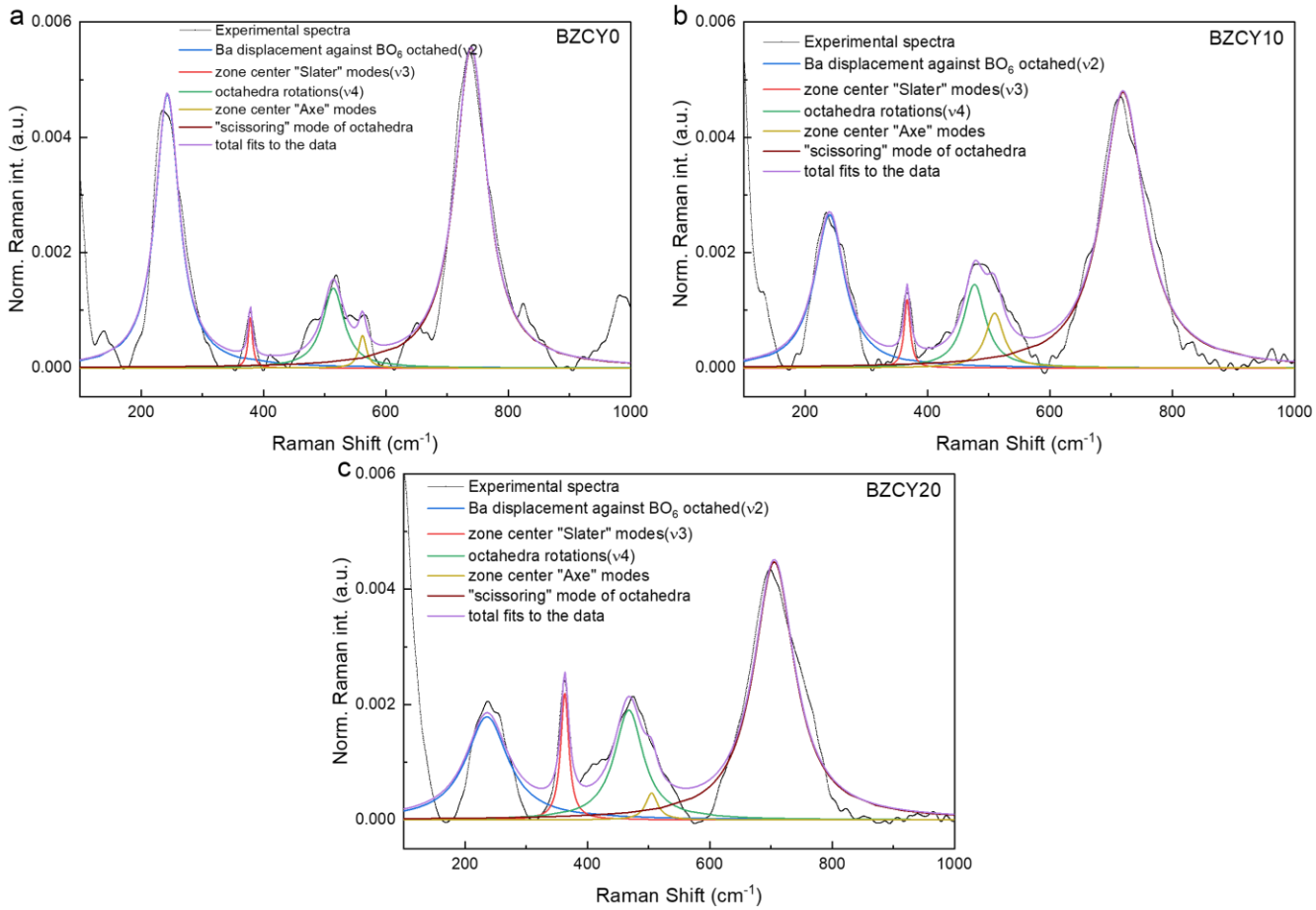

Figure S6. Fitting details of the Raman spectra of bulk BZCY. (a) BZCY0. (b) BZCY10. (c) BZCY20. Black curve: experimental spectra; purple curve: total fits to the data; blue curve: ν_2; red curve: ν_3; green curve: ν_4; yellow curve: zone center “Axe" modes;[11] brown curve: “scissoring" mode of octahedra.[12]

Table S5. Fitting results for bulk BZCY

Bulk BZCY	*v*2			*v*3			*v*4			R^2
	Position	Area	FWHM	Position	Area	FWHM	Position	Area	FWHM	
BZCY0	242.9	0.35	47.2	378.5	0.02	8.7	514.2	0.09	42.3	0.908
	±0.4	±0.00	±1.0	±0.8	±0.00	±2.4	±1.3	±0.01	±4.0	
BZCY10	240.0	0.25	59.7	366.8	0.02	12.0	467.9	0.1	43.8	0.896
	±1.0	±0.01	±2.8	±1.0	±0.00	±2.83	±3.4	±0.03	±8.1	
BZCY20	235.9	0.24	83.6	363.1	0.05	16.3	467.8	0.17	57.8	0.893
	±2.2	±0.01	±6.9	±0.8	±0.01	±2.4	±3.0	±0.03	±8.2	

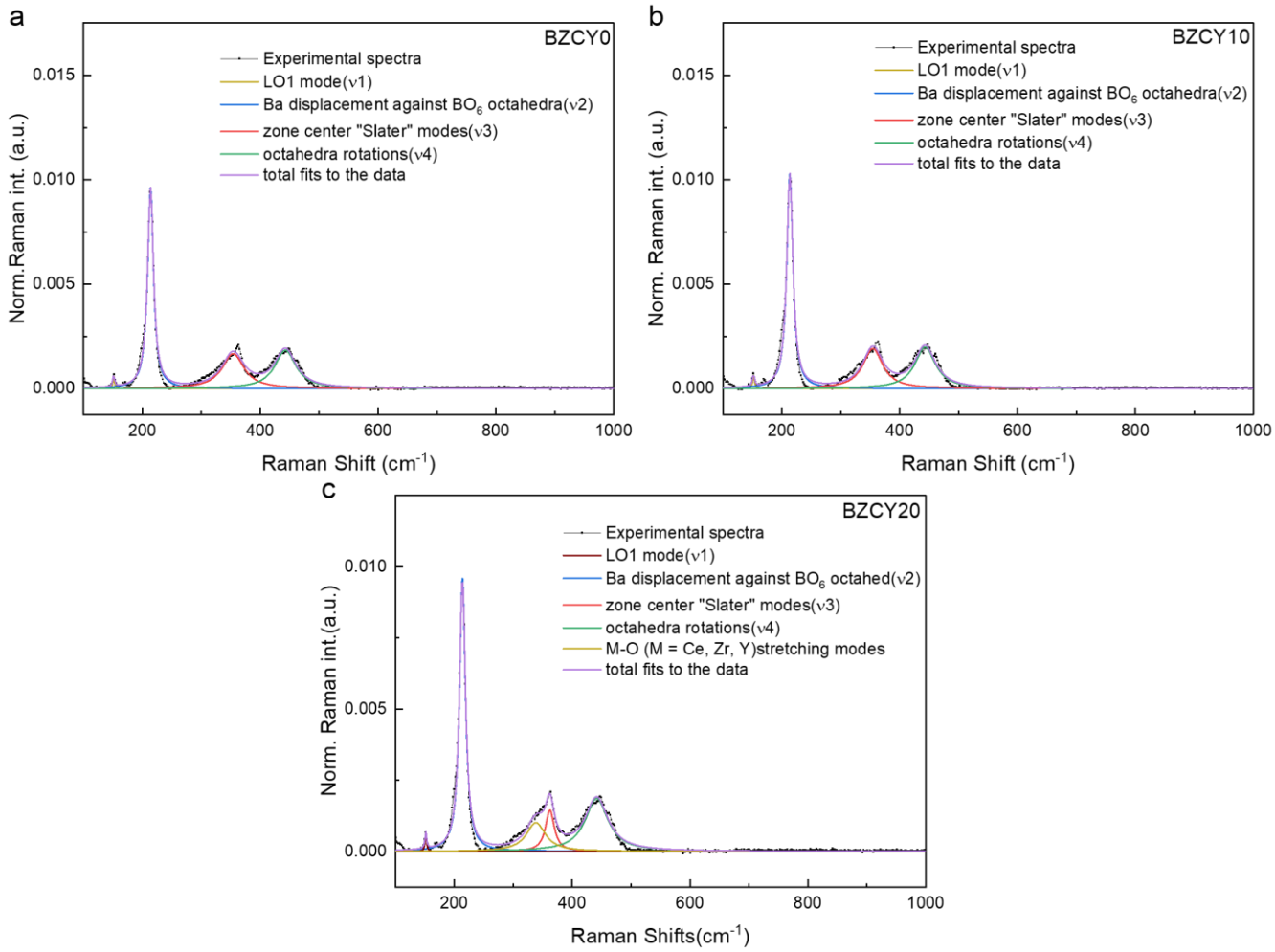

Figure S7. Fitting details of the Raman spectra of BZCY films. (a) BZCY0. (b) BZCY10. (c) BZCY20. Black curve: experimental spectra; purple curve: total fits to the data; blue curve: ν_2; red curve: ν_3; green curve: ν_4; yellow curve: LO1 mode.

Table S6. Fitting results for BZCY films

BZCY film	*v*2			*v*3			*v*4			R^2
	Position	Area	FWHM	Position	Area	FWHM	Position	Area	FWHM	
BZCY0	213.8	0.18	12.23	354.0	0.12	45.1	442.7	0.13	43.7	0.981
	±0.1	±0.00	±0.2	±0.7	±0.00	±2.1	±0.6	±0.00	±1.8	
BZCY10	213.6	0.20	12.67	354.4	0.12	41.1	443.1	0.13	42.8	0.976
	±0.1	±0.00	±0.2	±0.7	±0.00	±2.1	±0.6	±0.00	±2.0	
BZCY20	213.6	0.30	12.59	355.0	0.17	38.4	444.4	0.18	41.0	0.975
	±0.1	±0.00	±0.2	±0.6	±0.01	±2.0	±0.7	±0.01	±2.0	

To validate the characterization of local symmetry using relative intensity, this work also calculated the relative intensity between ν_2 and ν_4 and achieved the consistent trend, as shown in Figure S8.

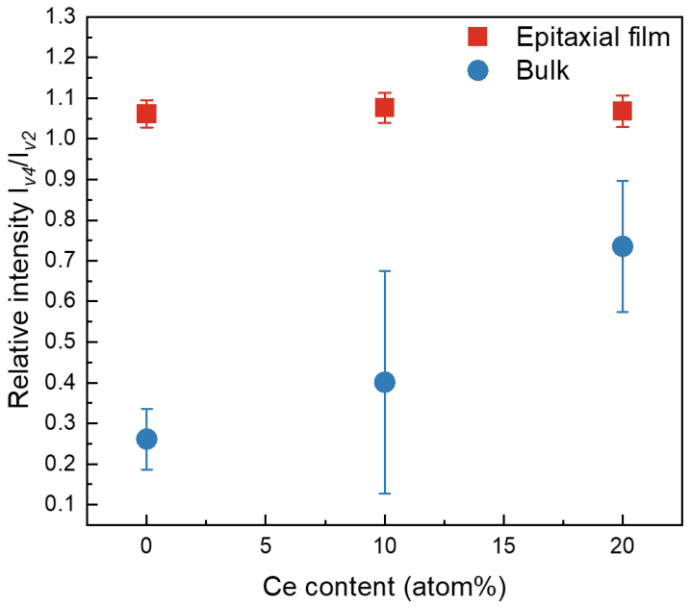

Figure S8. Raman relative intensity $I\nu_4/I\nu_2$ of BZCY epitaxial films and bulk samples with different Ce content. Difference between BZCY20 film and BZCY20 bulk is the smallest among all samples. The relative intensity is defined as octahedra rotations (ν_4)/ peak area of Ba displacement against BO_6 octahedra (ν_2).

5. XRD pattern of BZCY films with higher Ce content

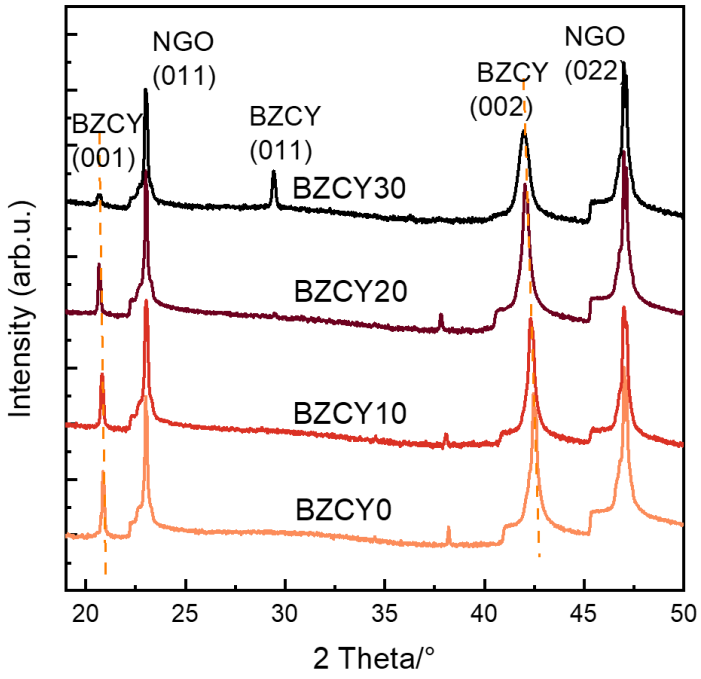

Figure S9. XRD patterns of BZCY films with different Ce content on NGO (110) substrate fabricated by PLD. The presence of a (011) reflection in the pattern of BZCY30 suggests a polycrystalline structure.

REFERENCES

1. J. H. Shim, T. M. Gür and F. B. Prinz, *Applied Physics Letters*, 2008, **92**, 253115.
2. Y. B. Kim, T. M. Gür, H.-J. Jung, S. Kang, R. Sinclair and F. B. Prinz, *Solid State Ionics*, 2011, **198**, 39-46.
3. A. Fluri, A. Marcolongo, V. Roddatis, A. Wokaun, D. Pergolesi, N. Marzari and T. Lippert, *Advanced science*, 2017, **4**, 1700467.
4. D. Pergolesi, E. Fabbri, A. D'Epifanio, E. Di Bartolomeo, A. Tebano, S. Sanna, S. Licoccia, G. Balestrino and E. Traversa, *Nature Materials*, 2010, **9**, 846-852.
5. H. Bae, Y. Lee, K. J. Kim and G. M. Choi, *Fuel Cells*, 2015, **15**, 408-415.
6. V. Foglietti, N. Yang, A. Tebano, C. Aruta, E. Di Bartolomeo, S. Licoccia, C. Cantoni and G. Balestrino, *Applied Physics Letters*, 2014, **104**, 081612.
7. Y. Wang, L. Wang, Y. Chen, X. Hu, Y. Yu and N. Yang, *The Journal of Physical Chemistry C*, 2023, **127**, 8937-8945.
8. A. Z. Samuel, R. Mukojima, S. Horii, M. Ando, S. Egashira, T. Nakashima, M. Iwatsuki and H. Takeyama, *ACS Omega*, 2021, **6**, 2060-2065.
9. H. M. N. Ullah, M. Rizwan, S. S. Ali, Z. Usman and C. Cao, *Materials Science and Engineering: B*, 2022, **286**, 116041.
10. J. Petzelt, T. Ostapchuk, I. Gregora, M. Savinov, D. Chvostova, J. Liu and Z. Shen, *Journal of the European Ceramic Society*, 2006, **26**, 2855-2859.
11. C. Toulouse, C. D. Amoroso, P. V. Xin, M. C. Hatnean, G. Balakrishnan, M. Maglione, P. Ghosez, J. Kreisel and M. Guennou, *Physical Review B*, 2019, **100**, 134102.
12. L. Mazzei, D. Rukser, F. Biebl, B. Grimm-Lebsanft, G. Neuber, D. Pergolesi, L. Börjesson, M. A. Rübhausen, J. Andreasson and M. Karlsson, *Journal of Physics: Condensed Matter*, 2020, **32**, 405403.